Cardamonin inhibits LPS-induced inflammatory responses and prevents acute lung injury by targeting myeloid differentiation factor 2

Libin Yang [a,1], Wu Luo [a,b,1], Qiuyan Zhang [a], Shanshan Hong [a], Yi Wang [a], Aleksandr V. Samorodov [c], Nipon Chattipakorn [d], Valentin N. Pavlov [c,**], Guang Liang [a,e,f,*]

[a] Chemical Biology Research Center, School of Pharmaceutical Sciences, Wenzhou Medical University, Wenzhou, Zhejiang 325035, China
[b] Medical Research Center, the First Affiliated Hospital, Wenzhou Medical University, Wenzhou, Zhejiang 325000, China
[c] Department of Pharmacology, Bashkir State Medical University, Ufa City 450005, Russia
[d] Cardiac Electrophysiology Research and Training Center, Faculty of Medicine, Chiang Mai University, Chiang Mai, Thailand
[e] School of Pharmaceutical Sciences, Hangzhou Medical College, Hangzhou, Zhejiang 311399, China
[f] Wenzhou Institute, University of Chinese Academy of Sciences, Wenzhou, Zhejiang 325001, China

ARTICLE INFO

ABSTRACT

Background: Acute lung injury (ALI) is a systemic inflammatory process, which has no pharmacological therapy in clinic. Accumulating evidence has demonstrated that natural compounds from herbs have potent anti-inflammatory efficacy in several disease models, which could be the potential candidates for the treatment of ALI.

Hypothesis/Purpose: Anti-inflammatory screening from natural product bank may provide new anti-inflammatory compounds for therapeutic target discovery and ALI treatment.

Methods: 165 natural compounds were screened for their anti-inflammatory activity in LPS-stimulated macrophages. PCR array, SPR and ELISA were used to determine the potential target of the most active compound, Cardamonin (CAR). The pharmacological effect of CAR was further evaluated in both LPS-stimulated macrophages and ALI mice model.

Results: Out of the screened 165 compounds, CAR significantly inhibited LPS-induced inflammatory cytokine secretion in macrophages. We further showed that CAR significantly inhibited NF-κB and JNK signaling activation, and thereby inflammatory cytokine production *via* directly interacting with MD2 *in vitro*. *In vivo*, our data show that CAR treatment inhibited LPS-induced lung damage, systemic inflammatory cytokine production, and reduced macrophage infiltration in the lungs, accompanied with reduced TLR4/MD2 complex in lung tissues, Treatment with CAR also dose-dependently increased survival in the septic mice induced by DH5α bacterial infection.

Conclusion: We demonstrate that a natural product, CAR, attenuates LPS-induced lung injury and sepsis by inhibiting inflammation *via* interacting with MD2, leading to the inactivation of the TLR4/MD2-MyD88-MAPK/NF-κB pathway.

Introduction

Acute lung injury (ALI) is an acute systemic inflammatory process. It is associated with prolonged mechanical ventilation, intensive medical care, high morbidity and mortality, and rising healthcare costs (Matthay et al., 2019). Patients with sepsis-induced ALI, which occurs due to an excessive response to infectious pathogens, particularly Gram-negative bacteria endotoxins such as lipopolysaccharide (LPS), have higher mortality rates than patients with other direct or indirect risk factors of ALI (Domscheit et al., 2020; Hudson et al., 1995). LPS has been used to induce ALI in animal models, which results in microvascular injury, diffused alveolar damage with intrapulmonary hemorrhage, edema, and fibrin deposition, (Chen et al., 2010; Johnson and Ward, 1974) all of which are features observed in ALI patients (Kabir et al., 2002). However, there are currently no pharmacological therapies available to treat ALI and its associated mortality effectively (Matthay et al., 2017). Majority of clinical trials with various pharmacologic strategies have not been successful, and accordingly, there is an urgent need to identify a pharmacologic strategy to reduce ALI-related mortality (Johnson and Matthay, 2010; Rubenfeld, 2015).

LPS-pattern recognition receptor, the Toll-like receptor 4 (TLR4), is widely expressed in the body, and binding of LPS to TLR4 evokes an innate inflammatory response in the body irrespective of the involvement of immune cells (Tapping et al., 2000; Yang et al., 1998). Another critical protein, myeloid differentiation 2 (MD2), associates with the extracellular domain of TLR4 following binding of LPS with TLR4 (Park et al., 2009). The LPS-TLR4-MD2 complex then initiate a signal transduction pathway that is mediated by the myeloid differentiation primary response gene 88 (MyD88) (Chen et al., 2020) and/or the TIR-domain-containing adapter-inducing IFN-β (TRIF) (Kenny and O'Neill, 2008). MyD88 activates the nuclear factor-κB (NF-κB) and MAPKs signaling pathways that lead to proinflammatory cytokine production (such as TNF-α and IL-6), which are involved in the pathogenesis of ALI (Matthay et al., 2017). These studies indicate an essential role of LPS/TLR4/MD2-mediated signaling in ALI, suggesting that the inhibition of this complex formation, *via* inhibiting MD2, might present a likely therapeutic target to treat or alleviate endotoxin- and/or sepsis-associated ALI.

Natural products are important source for new drug discovery. To screen for the drug that ameliorates inflammation in ALI, we screened 165 natural compounds stored in our natural compound bank for their anti-inflammatory activity, particularly by measuring their ability to inhibit IL-6 secretion (Supplementary Table S1). Among the screened 165 compounds, Cardamonin (CAR), which is a naturally occurring chalcone compound, stood out in the screening. CAR is commonly found in spices such as cardamom, and mainly isolated from different plants of the family Zingiberaceae and plants of genus *Syzygium*. CAR is isolated from rhizome of *Boesenbergia pandurata* and *B. rotunda, Alpenia pricei, Kaempferia parviflora*, and fruit and the rhizome of *Alpinia rafflesiana* and *A. conchigera* (Nawaz et al., 2020). CAR has been shown to have anti-inflammatory, antineoplastic, antioxidant, hypoglycemic, and anti-infectious activities (Goncalves et al., 2014; Nawaz et al., 2020). It is reported that the anti-inflammatory effect of CAR is mainly attributed to its inhibitory effect on NF-κB signaling pathway (Tan et al., 2021). However, the direct molecular targets of CAR contributing to its pharmacological effects are unclear. Here, we aimed to investigate the anti-inflammatory mechanism and target of CAR. We demonstrated that CAR elicits anti-inflammatory activities, restores lung and promotes survival in mice with LPS-induced ALI, *via* physically interacting with MD2 and inhibiting the TLR4-MD2 pathway.

Materials and methods

Reagents

CAR, with a purity > 98%, was purchased from Zhongke Quality Inspection (Cat. #19309-14-9, Beijing, China). LPS was obtained from Sigma-Aldrich (St. Louis, MO, USA). Antibodies against p38 (Cat. #9212S), p-p38 (Cat. #9211S), JNK (Cat. #9252S), p-JNK (Cat. #4668S), ERK (Cat. #4695S), p-ERK (Cat. #4695S), p-p65 (Cat. #3033), IκB-α (Cat. #4812S), and GADPH (#5174) were purchased from Cell Signaling Technology (Danvers, MA, USA). Antibodies against NF-κB P65 (Cat. #8008), TLR4 (Cat. #293072), MD2 (Cat. #80183), CD68 (Cat. #20060), and F4/80 (Cat. #377009) were purchased from Santa Cruz Biotechnology (Dallas, TX, USA). IL-6 antibody was obtained from proteintech (Cat. #66146-1-lg, Wuhan, China). Recombinant human MD2 (rhMD2) protein was obtained from R&D Systems (Cat. #1787-MD-050/CF, Minneapolis, MN, USA). Recombinant human TLR4 (ECD) protein (Cat. #10146-H08B, ECD, His Tag) was purchased from Sinobiological lnc. (Beijing, China). Mouse TNF-α (Cat. #85-88-7324-76) and IL-6 (Cat. #85-88-7064-76) ELISA kits were obtained from eBioscience (San Diego, CA, USA).

Cell isolation and culture

Mouse primary peritoneal macrophages (MPMs) were prepared from C57BL/6 mice as previously described (Chen et al., 2019). Primary cells were seeded in wells at a density of 10^6 cells/ml in RPMI-1640 medium with 10% FBS. Stably expressing NFκB-RE-EGFP reporter RAW264.7 cell lines (RAW264.7-NFκB-RE-EGFP) were kept in our laboratory and cultured in MEM-α medium containing 10% FBS and 0.1 μg/ml puromycin. RAW264.7-NFκB-RE-EGFP cell lines were carried out as described previously (Chen et al., 2019).

Surface plasmon resonance analysis

The binding affinity of CAR with rhMD2 and rhTLR4 protein was determined using a Biacore T200 instrument (GE Healthcare Inc., Piscataway, NJ, USA) with a CM7 sensor chip (GE. Cat #29-1470-20). Briefly, proteins were loaded to the sensors using the Amine coupling kit (GE. Cat. #BR-1000-50, GE Life Sciences). The CAR samples at indicated concentration were prepared with running buffer (PBS, 0.5% P20 and 5% DMSO). Sensor and sample plates were placed on the instrument, and then the CAR samples flowed over the target sensors. Eleven concentrations were injected successively at a flow rate of 30 μl/min for a 180 s association phase, which was followed by a 270 s dissociation phase at 25 °C. The final graphs were obtained by subtracting blank sensor grams and blank sample from the duplex. Data were analyzed with Biacore™ T200 software EV. KD was calculated by global fitting of the kinetic data from various concentrations of CAR using a 1:1 Langmuir binding model.

LPS displacement assay

The ability of CAR to interfere with LPS binding to rhMD2 was determined using a cell-free assay. Blocking on 96-well plates was performed with 3% BSA at 4 °C overnight. Then the plate was washed with PBST and 500 μg/ml LPS was added and incubated for 1 hour at room temperature. At the same time, rhMD2 was added at 1 μg/ml in 10 mM Tris-HCl buffer (pH 7.5), and rhMD2 was pre-incubated with a certain concentration of CAR (1, 10, 50 and 100 μM) on a shaker for 1 h. After washing with PBST, 10 mM Tris-HCl buffer (pH 7.5) containing 1 μg/ml rhMD2, and rhMD2-CAR premix were added, and incubated at room temperature for 2 h. After washing with PBST, MD2 antibody was added and incubated for 2 h at room temperature. After washing with PBST, HRP labeled secondary antibody were added and incubated at room temperature for 1 h. HRP activity was then determined in SpectraMax M5 (Molecular Devices, Sunnyvale, CA, USA) at 450 nm after the addition of TMB substrate (eBioscience).

Molecular docking of CAR to MD2

The molecular docking simulation was performed using AutoDock version 4.2.6. The crystal structure of human MD2 lipid IVa complex (PDB code 2E59) was obtained from Protein Data Bank. The AutoDock Tools version 1.5.6 package was applied to generate the docking input files and to analyze the docking results. A $60 \times 60 \times 60$-point grid box with a spacing of 0.375 Å between the grid points was implemented. The affinity maps of MD2 were calculated by AutoGrid. One hundred Lamarckian genetic algorithm runs with default parameter settings were processed. We then analyzed hydrogen bonds and bond lengths within the interactions of complex protein–ligand conformations.

Bis-ANS fluorescence displacement assays

5 μM 4,4′-Bis(phenylamino)-[1,1′-binaphthalene]-5,5′-disulfonic acid (bis-ANS, Cat. #5908/10, Carlsbad, CA, USA) and 5 nM rhMD2 were mixed in PBS and allowed to reach stable fluorescence under excitation at 385 nm. CAR, at indicated concentrations, was then added for 5 min, and relative fluorescence units emitted at 440–570 nm were measured. CAR was tested at indicated concentrations. Finally, fluorescence measurements were performed with SpectraMax M5 at 25 °C in 5 nm path-length quartz cuvettes.

Mouse model of acute lung injury (ALI)

All animal care and experimental procedures were approved by the Wenzhou Medical University Animal Policy and Welfare Committee (Approval Number: wydw2019-0439), and all animal experiments conform the NIH guidelines. Forty 7-week-old male C57BL/6 mice (weighing 19–21 g) were obtained from GemPharmatech Co., Ltd. (Nanjing, China). All animals were housed at a constant room temperature with a 12:12 h light/dark cycle and given food and water. The animals were acclimatized to the laboratory for 7 days before initiating the studies. All animal experiments were performed and analyzed by blinded experimenters. Randomization were used when dividing the groups. Each mouse was assigned a temporary random number within the weight range, and were then given their permanent numerical designation in the cages. For each group, a cage was selected randomly from the pool of all cages. Finally, mice were randomly divided into 5 groups ($n = 8$ *per* group).

The groups consisted of vehicle control mice (CON, with the same volume of 0.9% NaCl), LPS-induced ALI mice (LPS), mice treated with only 20 mg/kg CAR (CAR 20), LPS-induced ALI mice treated with 10 mg/kg CAR (LPS + CAR 10), LPS-induced ALI mice treated with 20 mg/kg CAR (LPS + CAR 20). CAR (dissolved in 0.5% CMC-Na) was administrated by oral gavage at 30 min before intratracheal instillation of LPS. CON and LPS groups received the same volume of 0.5% CMC-Na during this period. After LPS challenged for 6 h, Mice were sacrificed under 0.2 ml sodium pentobarbital anesthesia (100 mg/ml) i.p. injection. Serum, bronchoalveolar lavage fluid (BALF) and lung tissue samples were collected and stored at −80 °C. These sections were then dried at 60 °C for > 48 h and weighed again to obtain the dry lung weight. The ratio of the wet lung weight to the dry lung weight was calculated to assess lung edema. Portions of unirrigated lung sections were fixed in 4% formalin and embedded in paraffin for histological analysis. The remaining unirrigated lung tissues were used for RNA isolation and protein lysate preparation.

Bronchoalveolar lavage fluid (BALF) preparation and analysis

A tracheal cannula was inserted into the primary bronchus, and BALF was performed through the cannula by using Ca^{2+}/Mg^{2+}-free PBS. Approximately 0.8 ml BALF was acquired and centrifuged at $1000 \times g$ for 15 min at 4 °C. The supernatant was immediately stored at −80 °C for protein concentration and cytokines determination. The sediment

was resuspended in 50 μl 0.9% saline for determining the total number of cells and neutrophil count. Total cell number was acquired by use of a hemocytometer. Neutrophil count was acquired by counting 200 cells on a smear prepared by Wright–Giemsa stain (Nanjing Jiancheng Bioengineering Institute, Nanjing, China).

Western blotting

Cells or tissue were lysed by RIPA, and total protein was collected. The Bradford assay (Bio-Rad, Hercules, CA, USA) was used to detect the total protein concentration. After being boiled in loading buffer (Cat. #FD006, Hangzhou FUDE biological Technology) at 100 °C for 10 min, protein samples were separated by 10% SDS-PAGE and transferred onto a PVDF membrane (Bio-Rad). Membranes were blocked with 5% non-fat milk in Tris-buffered saline containing 0.05% Tween 20 (TBST) for 1.5 h at room temperature. The membranes were incubated with primary antibodies overnight at 4 °C. The membranes were then washed in TBST and reacted with HRP-conjugated secondary antibodies (1:10000) for 1 h at room temperature. Blots were then visualized using an enhanced chemiluminescence reagent (Bio-Rad Laboratories, Hercules, CA, USA). The density of the immunoreactive bands were analyzed using ImageJ software (NIH, Bethesda, MD, USA).

Immunoprecipitation assay to detecting MD2–TLR4 complexes

Cells or tissues were lysed with an extraction buffer containing mammalian protein extraction reagent, supplemented with protease and phosphatase inhibitor cocktails. Lysates were prepared from lung tissues as well. Samples were centrifuged at $15,000 \times g$ for 10 min at 4 °C. A sufficient amount of TLR4 antibody was added to 500 μg protein, and samples were gently rotated at 4 °C overnight. The immune complexes were precipitated with protein A + G agarose, and the precipitates were washed four times with ice-cold PBS. Finally, the proteins were then released by boiling in sample buffer, followed by Western blot analysis as described above.

Myeloperoxidase activity assay

To quantify neutrophil infiltration, myeloperoxidase (MPO, Cat. #A044) activity in the homogenized lung tissues were determined by using an MPO Detection Kit (Nanjing Jiancheng Bioengineering Institute, Nanjing, China). Total protein content in the samples were analyzed using total protein assay. MPO activity of lung tissues was presented as U/g protein.

Assay of cellular NF-κB p65 translocation

Levels of p-p65 were then probed using Western blotting. In addition, NF-κB activation was assessed by staining cells for p65 translocation using a Cellular NF-κB p65 Translocation Kit (Cat. #SN368, Beyotime Biotech, Shanghai, China) following manufacturer's protocol.

Enzyme-linked immunosorbent assay (ELISA)

Culture media were collected and used to measure TNF-α and IL-6 levels using ELISA. The levels of TNF-α and IL-6 in serum and BALF samples obtained from mice were also determined using the ELISA kits. Data was normalized to the amounts of total proteins from lysates of the same culture and expressed as a percentage of the LPS group in cell-based experiments (or were expressed as a percentage of one of mice in LPS group in animal-based experiments).

Screening anti-inflammatory natural compounds in MPMs

MPMs were plated in 96-well plate at a density of 10^6 cells/ml overnight. Cells were pre-treated with fresh completed medium

containing 10 μM natural product (165 compounds, respectively) for 1 h, then challenged with LPS (final concentration 0.5 μg/ml) for 24 h. IL-6 level in the culture medium was measured by ELISA and was normalized by the total protein. The results are presented as IL-6 inhibition rate, compared to LPS group. In addition, MPMs plated in 96-well plate were treated with 10 μM natural product (165 compounds, respectively) for 24 h and then the MTT assay was performed to evaluate the cytotoxicity of compounds.

RNA extraction and real-time quantitative reverse transcription PCR assay

Cells ($> 10^6$) or lung tissues (approximately 20–30 mg) were homogenized in TRIZOL (Invitrogen, Carlsbad, CA) for RNA extraction. Total RNA concentration and the purity of the samples were measured using an ultraviolet-visible spectrophotometer nanodrop 2000 (Thermo Scientific, USA). The OD ratio of A260/A280 must ranging within 1.8–2.2. Real-time quantitative reverse transcription PCR (RT-qPCR) was performed using the M-MLV Platinum RT-qPCR Kit (Invitrogen, Carlsbad, CA). Real-time quantitative PCR was carried out using the Eppendorf Realplex4 instrument (Eppendorf, Hamburg, Germany). Primers of genes were obtained from Invitrogen and shown in the Supplementary Table S2. Transcript levels were normalized to β-actin reference gene.

Lung histopathology

Unirrigated lungs were fixed in 4% neutral Paraformaldehyde and embedded in paraffin. Lung tissues were sectioned at 5 μm thickness. Deparaffinized sections were stained with the commercial haematoxylin and eosin kit (Cat. #C0105S, Beyotime Biotech, Shanghai, China) to estimate the degree of lung injury by light microscopy. Sections were also stained for IL-6 and macrophage marker CD68, F4/80 (all at 1:200 primary antibody dilution). Briefly, deparaffinized sections were was performed using 10 mM sodium citrate buffer (pH 6.5) to retrieve antigen epitope. After blocking endogenous peroxidase with 3% H_2O_2, all sections were blocked in 5% BSA. Primary antibodies were applied, and slides were incubated overnight at 4 °C. HRP-conjugated secondary antibody (1:200 dilution; 1 h incubation) and DAB were used for detection. Immunoreactivity was measured by Image J software (NIH, Bethesda, MD, USA).

Bacterial infection and sepsis

Septic mouse model induced by bacterial infection has been established and used in previously studies (Pan et al., 2015; Wegiel et al., 2014). Briefly, *E. coli* strain DH5α was grown in Luria Broth (LB) media and bacterial cell density was determined OD_{600} using an ultraviolet-visible spectrophotometer (NanoDrop2000, Thermo Scientific) and the corresponding colony-forming units (CFUs) were determined on LB agar plates. Seven-week-old male mice were acclimated for one week and were randomly assigned to four groups ($n = 10$ *per* group). The groups consisted of vehicle control mice (CON), DH5α-induced septic mice (DH5α), DH5α-induced septic mice with CAR treatment at 10 mg/kg (DH5α + CAR 10), DH5α-induced septic mice with CAR treatment at 20 mg/kg (DH5α + CAR 20). At 30 min after CAR (dissolved in 0.5% CMC-Na) was administrated by oral gavage, mice were intraperitoneally injected with viable DH5α *E. coli* (2×10^9 CFU/mouse) in 0.5 ml of PBS. The CON group received vehicle intraperitoneal injection and 0.5% CMC-Na gavage. Mouse survival was monitored every 6 h for 2 days.

Statistical analysis

All experiments are randomized and blinded. The data and statistical analysis comply with the recommendations on experimental design and analysis in pharmacology (Curtis et al., 2018). All data are reported as mean ± SEM. Data shown are from 3 independent experiments for cellular studies and 8–10 mice *per* group for animal studies. GraphPad Prism 8.0 software (San Diego, CA, USA) was used for statistical analysis. One-way ANOVA followed by Dunnett's post hoc test was used when comparing more than two groups of data. $p < 0.05$ was considered significant in statistics. Post-tests were run if F achieved $p < 0.05$ and there was no significant variance in homogeneity.

Results

A screening among 165 natural compounds identified CAR as a strong anti-inflammatory molecule in mouse primary macrophages

The level of IL6, an important inflammatory cytokine, has been widely considered as an inflammatory and pathological marker of ALI (Matthay et al., 2017). In order to find the anti-inflammatory compounds among 165 natural compounds stored in our natural compound bank (Supplementary Table S1), we screened for their anti-inflammatory activity at 10 μM by measuring their ability to inhibit IL-6 secretion using ELISA assay in LPS-challenged MPMs. Out of 165 compounds, a compound known as CAR demonstrated a very strong inhibition against LPS-induced IL-6 secretion (Fig. 1A), without obvious cytotoxicity in MPMs (Fig. 1B). Structurally, CAR is a naturally occurring chalcone (Fig. 1C). We further validated the anti-inflammatory effect and identified an effective dose of CAR in cultured MPMs. ELISA demonstrated significantly higher IL-6 and TNF-α secretion in the media of LPS-treated MPMs, which were significantly inhibited by CAR treatment at 5, 10 or 20 μM in a dose-dependent manner (Fig. 1D and E). We next measured some cytokines at transcript levels by real-time qPCR assay. We confirmed a dose-dependent reduction in the transcript levels of IL-6 (Fig. 1F), TNF-α (Fig. 1G), IL-1β (Fig. 1H), intercellular adhesion molecule-1 (ICAM-1, Fig. 1I), and vascular cell adhesion molecule-1 (VCAM-1, Fig. 1J) in the LPS-treated MPMs, indicating that CAR inhibits the transcription of these inflammatory molecule genes. Overall, these findings demonstrate that CAR elicits an anti-inflammatory effect in cultured MPMs.

PCR array indicates that CAR directly targets MD2 in LPS-challenged MPMs

To investigate the anti-inflammatory mechanism of CAR in MPMs, we performed a PCR array for 120 inflammation-related genes on RNAs extracted from LPS-challenged MPMs. Our PCR array data demonstrated that CAR treatment significantly affected the expression of more than 60 inflammation-related genes (Fig. 2A). LPS is known to induce inflammation *via* the MD2/TLR4 > MyD88/TRIF cascades (Fig. 2B). We, therefore, next looked at the effect of CAR on the expression of MyD88-dependent and TRIF-dependent inflammatory cytokines in the significantly affected genes in the PCR array data. We observed that CAR not only inhibited the expression of MyD88-dependent inflammatory cytokines (*i.e.*, interleukins and TNFs), but also the expression of TRIF-dependent inflammatory cytokines [*i.e.*, type I interferons (IFNs); IFNG, IFNA1, IFNA2 and IFNB] (Fig. 2A). This prompted us to hypothesize that anti-inflammatory effect of CAR is mediated by its effect on the upstream molecules MD2 and TLR4. To test our hypothesis, we performed immunoprecipitation analysis. Our data showed that LPS induced MD2-TLR4 complex formation, which was reduced following pre-treatment of CAR at 20 μM (Fig. 2C). Next to evaluate, whether CAR directly and physically interacts with MD2 or TLR4, the binding affinity surface plasmon resonance (SPR) assay was performed using recombinant human MD2 and TLR4. These data show that CAR directly binds to both rhMD2 and rhTLR4 proteins. However, the CAR-MD2 interaction is significantly stronger (KD value: 10^{-8} M) than CAR-TLR4 (KD value: 10^{-4} M), indicating that CAR mainly targets MD2 (Fig. 2D and E). We then evaluated the effect of CAR on LPS-MD2 interaction and showed that CAR significantly reduced LPS-MD2 interaction in a dose-
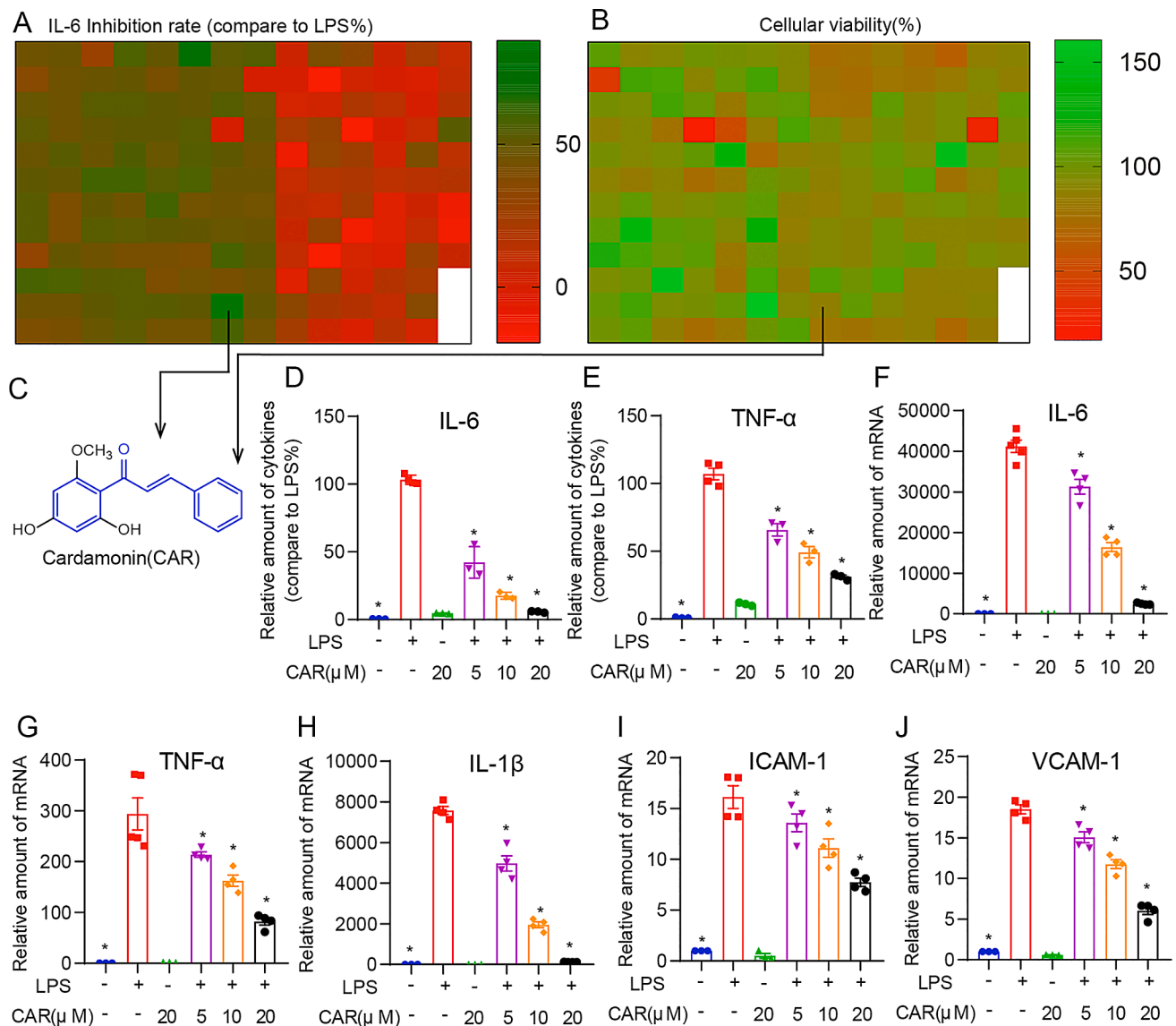
Fig. 1. CAR inhibited LPS-induced expression of inflammatory cytokines in MPMs. (A) MPMs were plated at a density of 10^6/plate overnight. Then cells were pretreated with 10 μM natural products library (165 compounds) for 1 h, then treated with LPS (0.5 μg/ml) for 24 h. IL-6 level in the culture medium was measured by ELISA and was normalized by the total protein. The results are presented as IL-6 inhibition rate, compared to LPS. CAR showed an inhibitory effect on IL-6 secretion in LPS-treated MPMs (indicated by arrow). (B) MPMs were plated at a density of 10^6/plate overnight. Then cells were exposed to 10 μM natural products library (165 compounds) for 24 h, MTT assay were evaluated cellular viability. (C) Chemical structure of CAR. MPMs were pretreated with CAR at 5, 10 or 20 μM for 1 h and then treated with LPS at 0.5 μg/ml for 24 h. DMSO was used as vehicle control for CAR. (D) IL-6 and (E) TNF-α cytokine levels in the culture medium were measured by ELISA. Data were normalized to total protein concentration from the same plate and presented as% of LPS group. The mRNA levels of inflammatory cytokines: (F) IL-6, (G) TNF-α, (H) IL-1β and adhesion molecules: (I) ICAM-1 and (J) VCAM-1 were measured by RT-qPCR. Data were normalized to β-actin and control group. Data is presented as mean ± SEM of three independent experiments; * $p < 0.05$ compared with LPS group.

dependent manner (Fig. 2F). The CAR-MD2 interaction was further confirmed by Bis-ANS fluorescence displacement assay (Fig. 2G). We were also able to demonstrate a putative CAR-MD2 binding site *in silico* using a docking software, which predicted Arg[90] and Gly[123] as important amino acid residues in CAR-MD2 interaction (Fig. 2H). Altogether, these data demonstrate that CAR physically interacts with MD2 and inhibits MyD88-dependent and TRIF-dependent inflammatory cytokines production in LPS-challenged MPMs, mainly *via* inhibiting LPS-MD2-TLR4 complex formation.

CAR inhibits LPS-induced MAPK and NF-κB activation in MPMs

LPS induced MD2/TLR4-mediated production of inflammatory cytokine is known to be arbitrated *via* activation of MAPKs and NF-κB

pathways. Our immunoblot data clearly demonstrate activation of JNK and p38 in LPS-treated MPMs; however, pre-treatment with all three doses of CAR were able to reduce the activation of JNK and p38 in a dose-dependent manner (Fig. 3A). Degradation of IκB and the phosphorylation of nuclear p65 are the essential steps for NF-κB activation and NF-κB-dependent transcription of inflammatory cytokines. LPS-induced IκB degradation and p65 phosphorylation were both inhibited in CAR-treated MPMs (Fig. 3B). In addition, LPS-induced p65 nuclear translocation was significantly reduced by CAR treatment to LPS-treated MPMs (Fig. 3C and D). These data were further confirmed in cells stably expressing NFκB-RE-EGFP reporter (RAW264.7-NFκB-RE-EGFP), which also showed increased nuclear green fluorescence indicating more nuclear transport or NF-κB activation in LPS-treated cells, which were significantly reduced in pre-treated cells with CAR in a dose-dependent
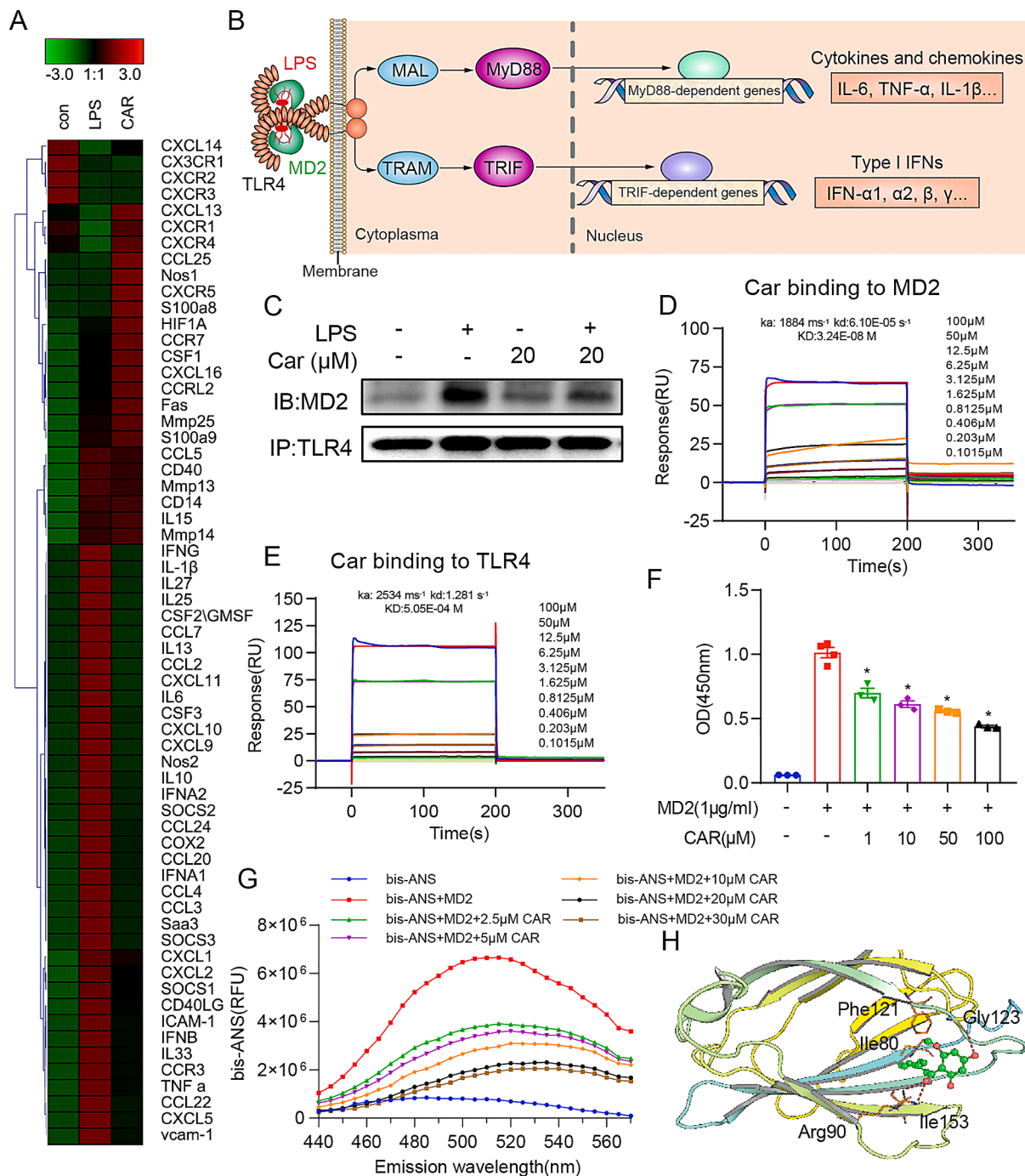
Fig. 2. CAR physically interacts with MD2 and inhibits both MyD88-dependent and TRIF-dependent inflammatory cytokines production in LPS-challenged MPMs. (A) Inflammation cytokine and receptor PCR array (120 genes). MPMs were pretreated with CAR at 20 μM for 1 h and then exposed to LPS for 6 h. Total RNAs were isolated and detected for the mRNA levels of 120 inflammation-related genes by qPCR. (B) Diagram depicting the LPS induced activation of TLR4/MD2 pathway and then either MyD88 and/or TRIF-dependent expression of inflammatory chemokines and cytokines. (C) MPMs were pretreated with CAR at 20 μM for 1 h and then exposed to LPS for 15 min. The complex of MD2–TLR4 was detected by immunoprecipitation. (D and E) The binding affinity of CAR with rhMD2 or rhTLR4 (ECD) was determined using an SPR assay. Increasing concentrations of CAR were mixed with rhMD2 or rhTLR4, and binding was determined. Association and dissociation constants are shown. (F) CAR reduced LPS binding to MD2. The LPS was coated on a 96-well plate blocked with AD, and different concentrations of cardamom and MD2 complexes were added. MD2 antibody, HRP labeled secondary antibody and TMB substrate was used to detect the substitution effect of different concentrations of CAR on LPS. Absorbance values at 450 nm are shown. (G) Bis-ANS fluorescence displacement assay to detect binding of CAR to MD2. Bis-ANS was incubated with rhMD2 to reach stable fluorescence under excitation at 380 nm. Different concentrations of CAR were added, and emission at 430–570 nm was detected. Data are shown as relative fluorescence units (RFU). (H) Molecular docking analysis of CAR to MD2. CAR (sticks-and-balls model) in the binding site of MD2 (cartoon). Data is presented as mean ± SEM of three separate experiments performed in duplicate; * $p < 0.05$ compared with LPS group.
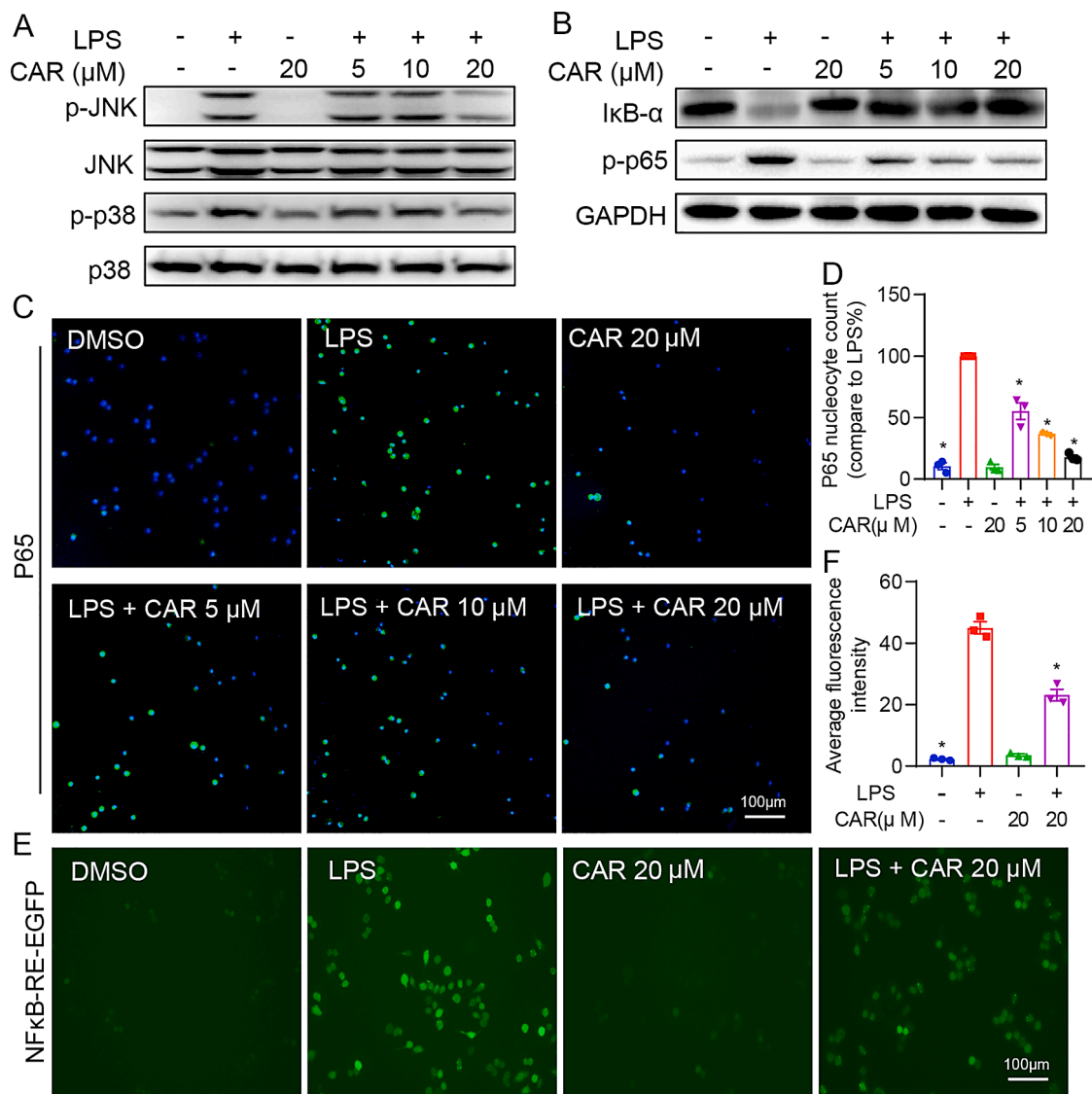
Fig. 3. CAR elicits its anti-inflammatory effects *via* inhibiting LPS-induced MAPK and NF-κB pathways. (A) MPMs were pretreated with CAR for 1 h followed by exposure to LPS for 15 min. The protein levels of p-JNK, JNK, p-p38, and p38 were examined by Western blot. (B–D) MPMs were pretreated with CAR for 1 h followed by LPS exposure for 30 min. (B) NF-κB activation was determined by measuring IκB and p-p65 levels. GAPDH was used as loading control. (C) P65 staining was carried out, and positivity was detected by Cy3-conjugated secondary antibody (Green). Cells were counterstained with DAPI (blue) (scale bar = 100 μm). (D) Quantification of p65 nucleocyte count for plane C. (E) RAW264.7 cells stably expressing NFκB-RE-EGFP reporter (RAW264.7-NFκB-RE-EGFP) were pretreated with CAR for 1 h followed by LPS exposure for 6 h. EGFP signal was detected by fluorescence microscope (scale bar = 100 μm) and (F) quantified. Data is presented as mean ± SEM of three separate experiments performed in duplicate; * $p < 0.05$ compared with LPS group. (For interpretation of the references to color in this figure legend, the reader is referred to the web version of this article.)

manner (Fig. 3E and F). These findings are in line with the anti-inflammatory effect of CAR *via* targeting MD2.

CAR protects against LPS-induced acute lung injury in mouse model

We tested the anti-inflammatory effects of CAR in a mouse model of LPS-induced ALI. Two test concentrations (10 and 20 mg/kg) were used to validate the effects of CAR. The doses were selected according to the previous studies on CAR (Lee et al., 2006). LPS-induced significant lung injury, which was evident by hypercellularity, alveolar walls thickening and disruption of the normal lung architecture, all of which were also restored in the CAR-treated mice (Fig. 4A). LPS-treatment was associated with increased lung injury and enhanced lung wet/dry ratio, which were also reduced in the CAR-treated mice (Fig. 4B and C). The protective effect of CAR was further evident in reduced protein concentration, reduced total cells, particularly reduced neutrophils, in the BALF

of CAR- and LPS-treated mice in comparison to LPS-treated mice (Fig. 4D–F). Furthermore, Myeloperoxidases (MPOs), which are released into extracellular fluid in the setting of inflammation in the lungs in ALI, were increased in LPS treated mice, while CAR-treatment significantly reduced the MPO activity (Fig. 4G). Fig. 4A–G showed slight dose-dependence of CAR in mice with ALI. These findings confirm the protective effect of CAR against LPS-induced ALI and support our *in vitro* findings, indicating the anti-inflammatory effect of CAR in the setting of LPS challenge.

CAR treatment inhibits MD2-TLR4 complex formation and inflammatory responses in LPS-induced ALI

We investigated the effect of CAR on the formation of the MD2-TLR4 complex *in vivo* in the lungs. Consistent with our *in vitro* data, CAR treatment dose-dependently inhibited the MD2-TLR4 complex
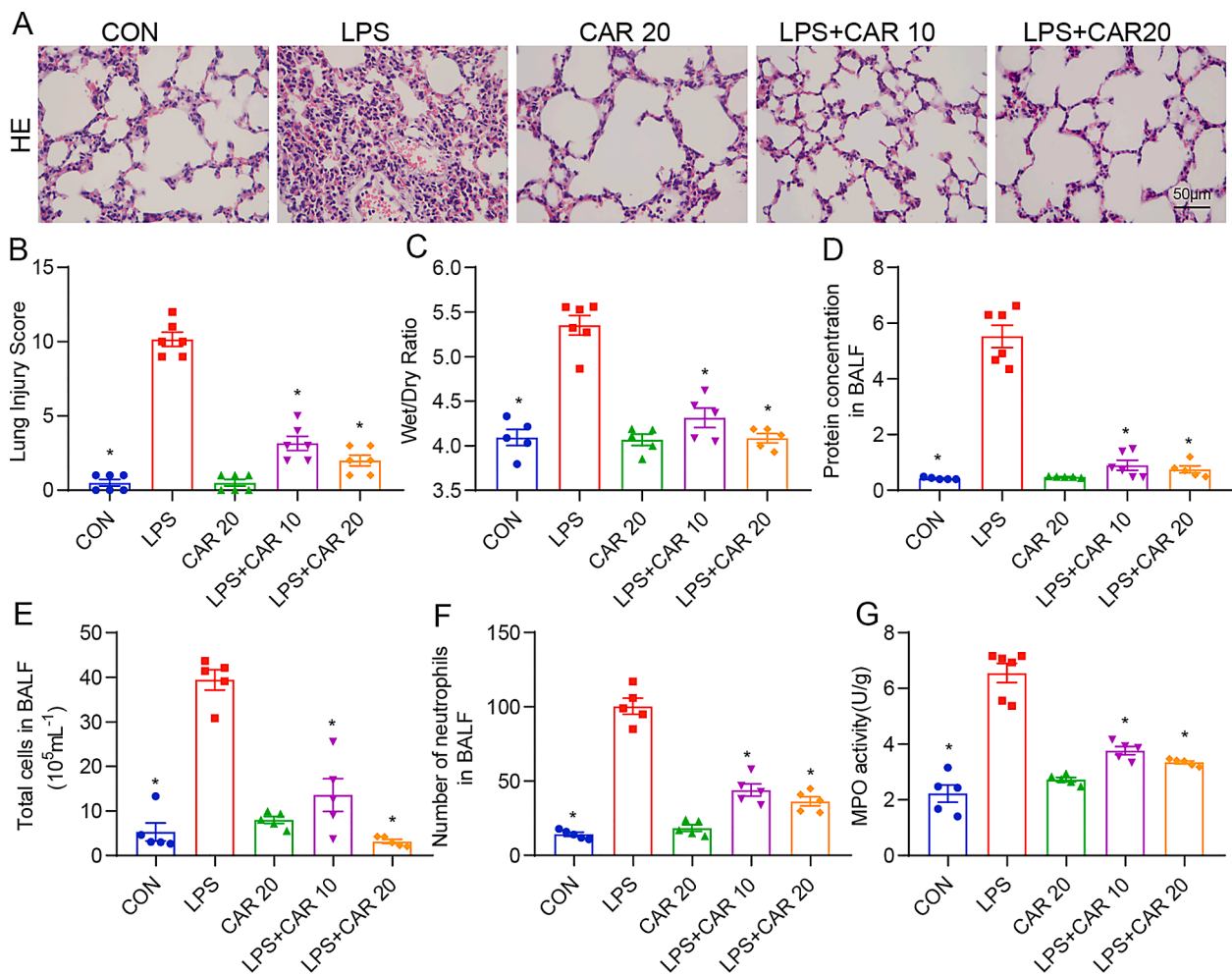
Fig. 4. CAR protects against LPS-induced acute lung injury in mouse model. (A) Representative histological images of lung tissues harvested from mice following LPS challenge 6 h. Tissues were stained with haematoxylin and eosin (scale bar = 50 μm). (B) Lung injury score as assessed by histological analysis of lung tissues. (C) Lung wet/dry ratio was determined at 6 h after LPS challenge. (D) BALF was collected 6 h after LPS challenge, and the amount of protein was measured by Bradford assay. (E, F) The numbers of (E) total cells and (F) neutrophils in BALF following LPS challenge. (G) CAR inhibited the LPS-induced MPO activity in lung tissue. Data are presented as mean ± SEM; n = 5–6 mice *per* group; * $p < 0.05$ compared with LPS group.

formation in the lungs of LPS-treated mice (Fig. 5A and B). Increased levels of inflammatory cytokines have been reported in the BALF and in the circulation of ALI patients. BALF of LPS-treated mice demonstrated significantly increased amount of IL-6 and TNF-α, which were diminished by the CAR treatment (Fig. 5C and D). LPS also induced increased circulatory IL-6 and TNF-α; however, CAR treatment significantly reduced the levels of circulatory IL-6 and TNF-α in LPS-treated mice (Fig. 5E and F). We also confirmed the anti-inflammatory effect of CAR on LPS-induced IL-6 production by lung tissue histochemical analysis (Fig. 5G and H). We also measured the transcript level of IL-6, TNF-α, and IL-1β in the lungs. As expected, our data demonstrate a significant induction of these cytokines by LPS, which were ameliorated by CAR treatment (Fig. 5I–K).

Next, to measure if CAR reduced macrophage infiltration, we performed immunohistochemical staining using macrophage-specific CD68 and F4/80 antibodies. Our data demonstrated a significant reduction in macrophage infiltration in the lungs of CAR- and LPS-treated mice in comparison to LPS-treated mice (Fig. 6A–D). Accordingly, our data also demonstrated increased expression of ICAM-1 and VCAM-1 in the lungs of LPS-treated mice, which were significantly inhibited in the CAR- and LPS-treated mice in comparison to LPS-treated mice (Fig. 6E and F). Taken together, our data demonstrate that CAR inhibits MD2-TLR4 complex formation and subsequent inflammatory responses in ALI model.

CAR promotes survival in septic mice

Finally, we looked at the anti-inflammatory effect of CAR on overall survival following infection (i.p.) with viable *E. coli*. Bacterial infection-induced mortality was significantly reduced in CAR-treated mice in a dose-dependent manner, where 10 mg/kg and 20 mg/kg doses of CAR were associated with more than 50% and 75% survival following sepsis, respectively (Fig. 7).

Discussion

Recently, chalcone, which has an anti-inflammatory, antineoplastic, antioxidant activity with the inherent advantage of occurring naturally, has received growing attention from the scientific community for its therapeutic application (Goncalves et al., 2014). Accordingly, CAR, which is a chalcone derivative, was shown to have an anti-inflammatory effect against LPS *via* NF-κB signaling in microglial cells (Chow et al., 2012). CAR has been tested in disease models previously, and there are reports (Chow et al., 2012; Hatziieremia et al., 2006; Lee et al., 2006, 2012; Takahashi et al., 2011) explaining the anti-inflammatory effect of CAR by its negative influence on the NF-κB signaling, which plays a crucial role in regulating immune responses to infection, particularly LPS-induced inflammation; TNF-α, IL-1 β and IL-6 release; and also intracellular reactive oxygen species generation (Ahmad et al., 2006;
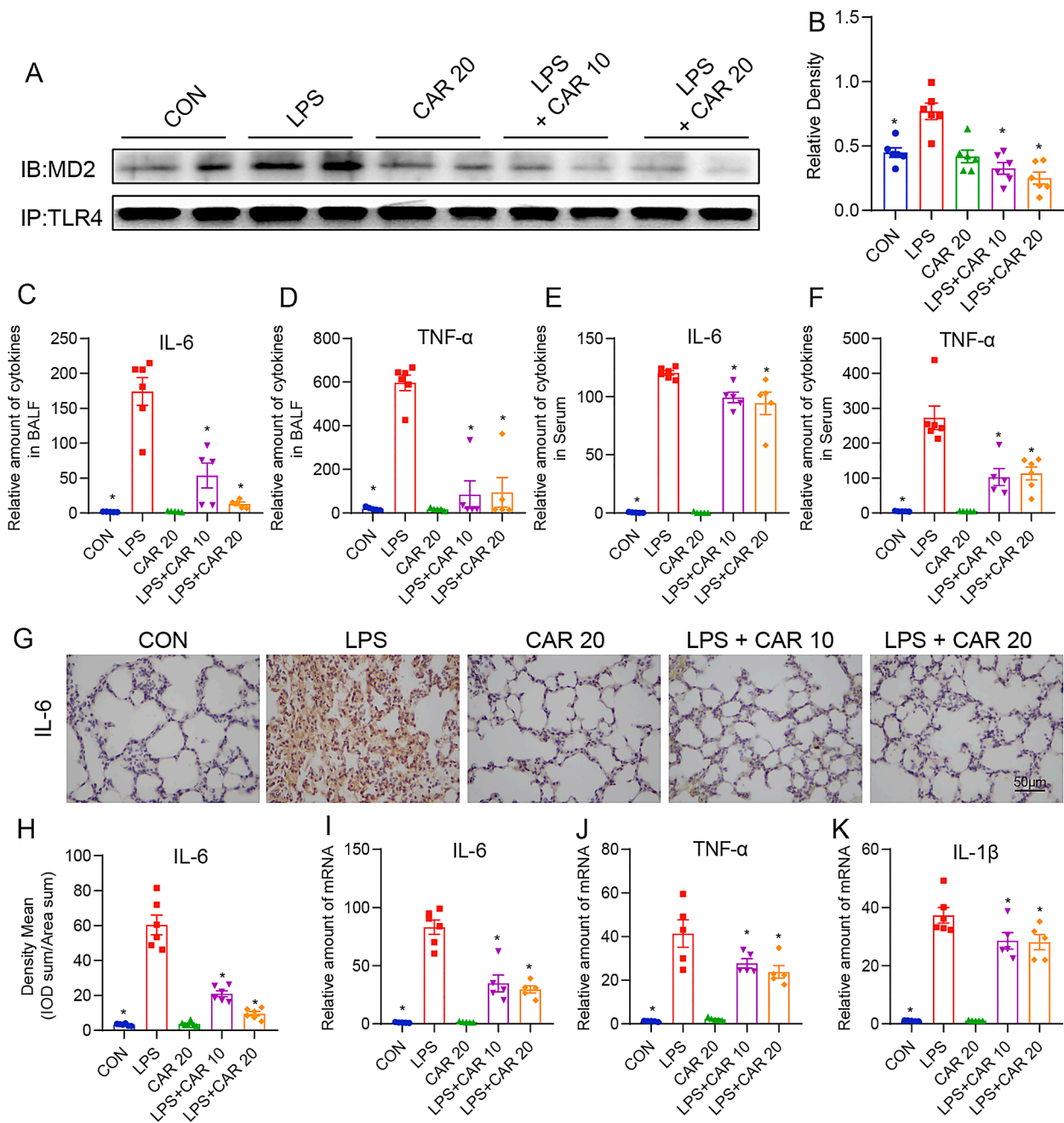
Fig. 5. CAR treatment inhibits MD2-TLR4 complex formation and production of inflammatory cytokines in the lungs in LPS-induced ALI. (A) The formation of MD2/TLR4 complex in lung tissues was detected by Co-IP. (B) Densitometric quantification of MD2/TLR4 complex levels. (C–F) Inflammatory cytokines in BALF and serum were detected by ELISA. BALF levels are shown in IL-6 (C) and TNF-α (D), and serum levels are shown in IL-6 (E) and TNF-α (F). (G) Immunohistochemical staining for IL-6 in lung tissues (scale bar = 50 μm). (H) Quantification of IL-6 positivity. Data are shown as ratio of positive staining area to total area. (I–K) Transcript levels of inflammatory cytokines (I) IL-6, (J) TNF-α, and (K) IL-1β in lung tissues of mice were determined by RT-qPCR. Data normalized to β-actin and data is presented as mean ± SEM; * $p < 0.05$ compared with LPS group ($n = 5$–6 mice *per* group). IOD, integral optical density.

Chow et al., 2012). A study by Wei et al. showed that CAR decreases systemic inflammatory responses during LPS-induced sepsis *via* down-regulating TNF-α and interleukins (IL-1β and IL-6) (Wei et al., 2012). MAPKs are also has been shown to be negatively regulated by CAR. Particularly relevant to the present work, CAR is shown to prevent endothelial barrier dysfunction *via* selectively inhibiting MAPK activation (Wei et al., 2012). Hatziieremia et al. demonstrated that CAR inhibits inflammatory cytokines in monocytes/macrophages by inhibiting the JNK and p38 MAPK pathways (Hatziieremia et al., 2006). In vascular smooth muscle cell CAR prevented function angiotensin II-induced dysfunction by inhibiting p38 activation (Shen et al., 2014). CAR's

anti-inflammatory activity in carrageenan-induced paw edema was attributed to inhibition of JNK signaling pathway by CAR (Li et al., 2015).

Ours is the first study to demonstrate that CAR elicits protection against LPS-induced ALI *via* targeting MD2. The overall aim of this study was to investigate the mechanism of the effects of CAR on LPS-induced pro-inflammatory responses and lung injury in mice. The key findings from our study are that CAR elicits its anti-inflammatory and protective effects against LPS-induced ALI by physically interacting and thereby inhibiting TLR4/MD2 complex, which is an essential step in LPS-induced inflammation. CAR-mediated inhibition of TLR4/MD2
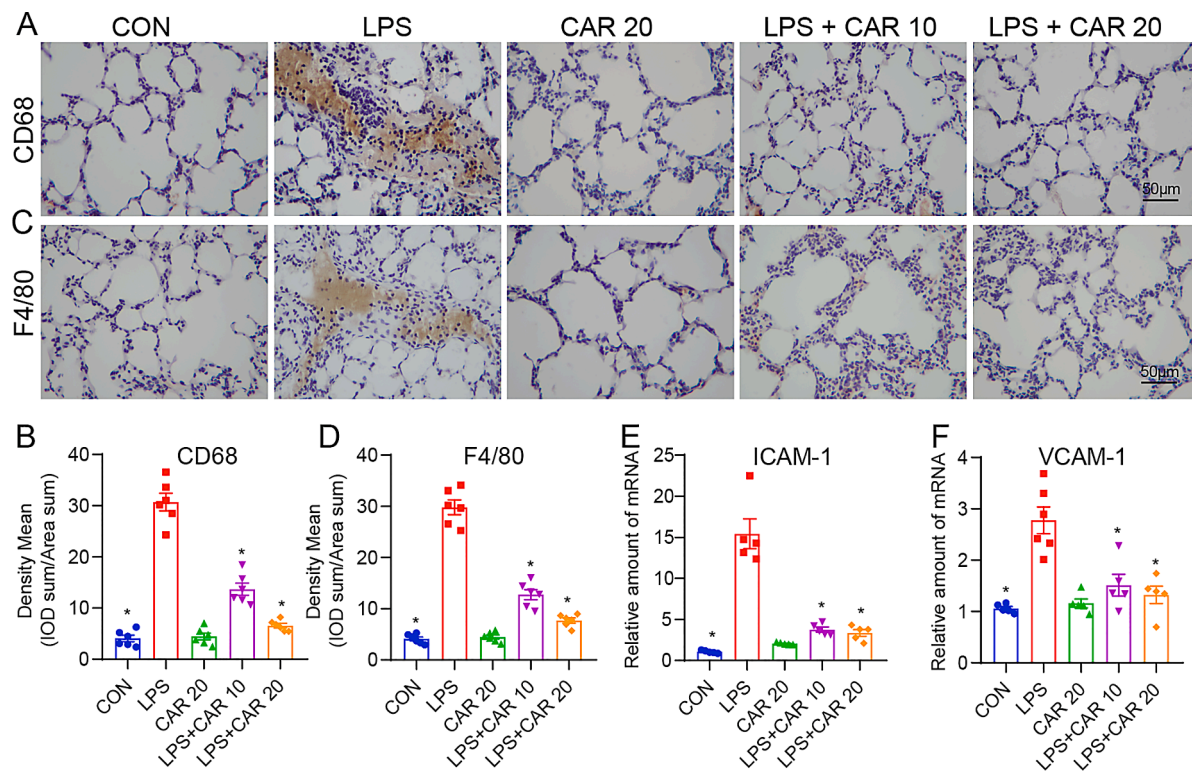
Fig. 6. CAR inhibits macrophage infiltration in the lungs in LPS-induced ALI. (A) Immunohistochemical staining for macrophage marker CD68 in lung tissues of mice challenged with LPS. Immunoreactivity is shown in brown (scale bar = 50 μm). (B) Quantification of CD68 positivity. Data are shown as ratio of positive staining area to total area. (C) Immunohistochemical staining for F4/80 in lung tissues (scale bar = 50 μm). (D) Quantification of F4/80 positivity. (E–F) Transcript levels of adhesion molecules (E) ICAM-1 and (F) VCAM-1 in lung tissues of mice were determined by RT-qPCR. Data normalized to β-actin and is presented as mean ± SEM; * $p < 0.05$ compared with LPS group (n = 5–6 mice *per* group). IOD, integral optical density.
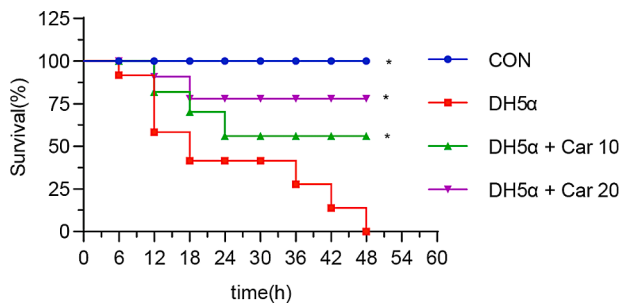

Fig. 7. CAR-treatment promotes survival in sepsis-induced ALI mouse models. C57BL/6 mice were orally administrated with CAR (10 and 20 mg/kg body weight) or vehicle (0.5% DMSO) prior to infection (i.p.) with viable *E. coli* DH5α (2×10^9 CFU/mouse). Mouse survival was monitored every 6 h for 2 days. Kaplan-Meier survival curves were used to analyze the data ($n = 10$/ group). The significance was evaluated by the log rank (Mantel-Cox) test. i.g., irrigation; i.p., intraperitoneal. * $p < 0.05$ compared with DH5α group.

complex formation was further associated with reduced NF-κB and MAPK activation and production of pro-inflammatory cytokines in cultured primary macrophages and in the lungs of LPS-treated mice *in vivo*. CAR-treatment also protected mice lungs against LPS-ALI-associated structural alterations and provided overall increased survival. Overall, our data indicate that CAR inhibits MD2/TLR4 pathway activation by targeting MD2, and that CAR may serve as a therapeutic target to treat ALI or ameliorate ALI-related adverse phenotypes.

It is well described that TLR4, along with its co-receptor MD2, mediate LPS-induced lung injury (Akashi et al., 2000; Qureshi et al., 2006; Shimazu et al., 1999). We investigated MD2 as the target of CAR using co-IP, SPR, displacement, and docking assays. Consistent with our

hypothesis, CAR not only physically interacted with MD2 but also weakened its biding with LPS preventing subsequent activation of the TLR4 pathway. The anti-inflammatory effect of CAR, most probably, is through its interaction with MD2 as the interaction between CAR and TLR4 was weaker in comparison to CAR with MD2; however, there is always a possibility of an additive effect of interaction between CAR and TLR4 on overall inhibition of inflammation. CAR is also shown to protect against LPS-induced septic shock, LPS-induced myocardial contractile dysfunctions, (Tan et al., 2021) and LPS-induced inflammatory response in microglial cells (Chow et al., 2012). A chalcone derivative, dimethyl CAR, exhibits anti-inflammatory effects *via* interfering with the PI3K-PDK1-PKCα signaling pathways, (Yu et al., 2015) which are not reported in LPS-induced ALI and therefore, we did not investigate these pathways in our ALI model. However, the PI3K-PDK1-PKCα pathway in ALI and the protective effect of CAR cannot be ruled out and need to be investigated in the future.

The critical role played by MD2 in ALI can be understood by the fact that LPS nasal challenge does not elicit pulmonary inflammation in systemic MD2 knockout mice (Hadina et al., 2008). It is also established that inhibition of MD2 inhibits inflammatory diseases that include sepsis, (Duan et al., 2014) lung inflammation (Hadina et al., 2008) and asthma (Hosoki et al., 2016). We recently demonstrated that inhibition of MD2, thereby MD2-TLR4 complex formation by a naphthoquinone compound Shikonin significantly reduced LPS-induced production of pro-inflammatory cytokines, macrophage infiltration and lung edema (Zhang et al., 2018). These findings strengthen the idea that MD2 inhibition is a potential therapeutic target to treat ALI and sepsis.

Conclusion

Our studies, for the first time, report that CAR interacts with MD2, inhibiting overall LPS-MD2-TLR4 interaction and thereby preventing

downstream MyD88 and/or TRIF-mediated activation of NF-κB and MAPK signaling and inflammatory chemokine and cytokine production and therefore reducing inflammation and providing protection in ALI. Overall, our findings present an interesting idea to utilize the ability of CAR to bind and inhibit MD2 as a therapeutic option to treat ALI and warrants future drug discovery.

Authors' contribution

Guang Liang, Valentin N. Pavlov, Nipon Chattipakorn, and Yi Wang: conception and design, manuscript writing; Libin Yang, Wu Luo, Qiuyan Zhang, and Shanshan Hong: experiments, collection, analysis and interpretation of data; Yi Wang, Valentin N. Pavlov, and Guang Liang: collection, interpretation and analysis of data; Guang Liang and Wu Luo: interpretation of data, manuscript revision. All data were generated in-house, and no paper mill was used. All authors agree to be accountable for all aspects of work ensuring integrity and accuracy.

CRediT authorship contribution statement

Libin Yang: Investigation, Data curation, Methodology, Writing – original draft. **Wu Luo:** Investigation, Data curation, Methodology, Writing – original draft. **Qiuyan Zhang:** Investigation, Data curation, Methodology, Writing – original draft. **Shanshan Hong:** Investigation, Data curation, Methodology, Writing – original draft. **Yi Wang:** Resources, Formal analysis, Writing – review & editing. **Aleksandr V. Samorodov:** Resources, Formal analysis, Writing – review & editing. **Nipon Chattipakorn:** Conceptualization, Project administration, Funding acquisition, Supervision, Writing – original draft. **Valentin N. Pavlov:** Conceptualization, Project administration, Funding acquisition, Supervision, Writing – original draft. **Guang Liang:** Conceptualization, Project administration, Funding acquisition, Supervision, Writing – original draft.

Declaration of Competing Interest

We confirm that there is no conflict of interest associated with this publication and there is no significant financial support for this work that could have influenced its outcome.

Acknowledgments

Supplementary materials

Supplementary material associated with this article can be found, in the online version, at doi:10.1016/j.phymed.2021.153785.

References

Ahmad, S., Israf, D.A., Lajis, N.H., Shaari, K., Mohamed, H., Wahab, A.A., Ariffin, K.T., Hoo, W.Y., Aziz, N.A., Kadir, A.A., Sulaiman, M.R., Somchit, M.N., 2006. Cardamonin, inhibits pro-inflammatory mediators in activated RAW 264.7 cells and whole blood. Eur. J. Pharmacol. 538, 188–194.

Akashi, S., Shimazu, R., Ogata, H., Nagai, Y., Takeda, K., Kimoto, M., Miyake, K., 2000. Cutting edge: cell surface expression and lipopolysaccharide signaling *via* the toll-like receptor 4-MD-2 complex on mouse peritoneal macrophages. J. Immunol. 164, 3471–3475.

Chen, H., Bai, C., Wang, X., 2010. The value of the lipopolysaccharide-induced acute lung injury model in respiratory medicine. Expert Rev. Respir. Med. 4, 773–783.

Chen, L., Chen, H., Chen, P., Zhang, W., Wu, C., Sun, C., Luo, W., Zheng, L., Liu, Z., Liang, G., 2019. Development of 2-amino-4-phenylthiazole analogues to disrupt myeloid differentiation factor 88 and prevent inflammatory responses in acute lung injury. Eur. J. Med. Chem. 161, 22–38.

Chen, L., Zheng, L., Chen, P., Liang, G., 2020. Myeloid differentiation primary response protein 88 (MyD88): the central hub of TLR/IL-1R signaling. J. Med. Chem. 63, 13316–13329.

Chow, Y.L., Lee, K.H., Vidyadaran, S., Lajis, N.H., Akhtar, M.N., Israf, D.A., Syahida, A., 2012. Cardamonin from *Alpinia rafflesiana* inhibits inflammatory responses in IFN-gamma/LPS-stimulated BV2 microglia *via* NF-kappaB signalling pathway. Int. Immunopharmacol. 12, 657–665.

Curtis, M.J., Alexander, S., Cirino, G., Docherty, J.R., George, C.H., Giembycz, M.A., Hoyer, D., Insel, P.A., Izzo, A.A., Ji, Y., MacEwan, D.J., Sobey, C.G., Stanford, S.C., Teixeira, M.M., Wonnacott, S., Ahluwalia, A., 2018. Experimental design and analysis and their reporting II: updated and simplified guidance for authors and peer reviewers. Br. J. Pharmacol. 175, 987–993.

Domscheit, H., Hegeman, M.A., Carvalho, N., Spieth, P.M., 2020. Molecular dynamics of lipopolysaccharide-induced lung injury in rodents. Front. Physiol. 11, 36.

Duan, G., Zhu, J., Xu, J., Liu, Y., 2014. Targeting myeloid differentiation 2 for treatment of sepsis. Front. Biosci. 19, 904–915.

Goncalves, L.M., Valente, I.M., Rodrigues, J.A., 2014. An overview on cardamonin. J. Med. Food 17, 633–640.

Hadina, S., Weiss, J.P., McCray Jr., P.B., Kulhankova, K., Thorne, P.S., 2008. MD-2-dependent pulmonary immune responses to inhaled lipooligosaccharides: effect of acylation state. Am. J. Respir. Cell Mol. Biol. 38, 647–654.

Hatziieremia, S., Gray, A.I., Ferro, V.A., Paul, A., Plevin, R., 2006. The effects of cardamonin on lipopolysaccharide-induced inflammatory protein production and MAP kinase and NFkappaB signalling pathways in monocytes/macrophages. Br. J. Pharmacol. 149, 188–198.

Hosoki, K., Boldogh, I., Aguilera-Aguirre, L., Sun, Q., Itazawa, T., Hazra, T., Brasier, A.R., Kurosky, A., Sur, S., 2016. Myeloid differentiation protein 2 facilitates pollen- and cat dander-induced innate and allergic airway inflammation. J. Allergy Clin. Immunol. 137, 1506–1513 e1502.

Hudson, L.D., Milberg, J.A., Anardi, D., Maunder, R.J., 1995. Clinical risks for development of the acute respiratory distress syndrome. Am. J. Respir. Crit. Care Med. 151, 293–301.

Johnson, E.R., Matthay, M.A., 2010. Acute lung injury: epidemiology, pathogenesis, and treatment. J. Aerosol. Med. Pulm. Drug Deliv. 23, 243–252.

Johnson, K.J., Ward, P.A., 1974. Acute immunologic pulmonary alveolitis. J. Clin. Invest. 54, 349–357.

Kabir, K., Gelinas, J.P., Chen, M., Chen, D., Zhang, D., Luo, X., Yang, J.H., Carter, D., Rabinovici, R., 2002. Characterization of a murine model of endotoxin-induced acute lung injury. Shock 17, 300–303.

Kenny, E.F., O'Neill, L.A., 2008. Signalling adaptors used by toll-like receptors: an update. Cytokine 43, 342–349.

Lee, J.H., Jung, H.S., Giang, P.M., Jin, X., Lee, S., Son, P.T., Lee, D., Hong, Y.S., Lee, K., Lee, J.J., 2006. Blockade of nuclear factor-kappaB signaling pathway and anti-inflammatory activity of cardamomin, a chalcone analog from *Alpinia conchigera*. J. Pharmacol. Exp. Ther. 316, 271–278.

Lee, M.Y., Seo, C.S., Lee, J.A., Shin, I.S., Kim, S.J., Ha, H., Shin, H.K., 2012. Alpinia katsumadai H(AYATA) seed extract inhibit LPS-induced inflammation by induction of heme oxygenase-1 in RAW264.7 cells. Inflammation 35, 746–757.

Li, Y.Y., Huang, S.S., Lee, M.M., Deng, J.S., Huang, G.J., 2015. Anti-inflammatory activities of cardamonin from Alpinia katsumadai through heme oxygenase-1 induction and inhibition of NF-kappaB and MAPK signaling pathway in the carrageenan-induced paw edema. Int. Immunopharmacol. 25, 332–339.

Matthay, M.A., McAuley, D.F., Ware, L.B., 2017. Clinical trials in acute respiratory distress syndrome: challenges and opportunities. Lancet Respir. Med. 5, 524–534.

Matthay, M.A., Zemans, R.L., Zimmerman, G.A., Arabi, Y.M., Beitler, J.R., Mercat, A., Herridge, M., Randolph, A.G., Calfee, C.S., 2019. Acute respiratory distress syndrome. Nat. Rev. Dis. Primers 5, 18.

Nawaz, J., Rasul, A., Shah, M.A., Hussain, G., Riaz, A., Sarfraz, I., Zafar, S., Adnan, M., Khan, A.H., Selamoglu, Z., 2020. Cardamonin: a new player to fight cancer *via* multiple cancer signaling pathways. Life Sci. 250, 117591.

Pan, H., Xu, L.H., Huang, M.Y., Zha, Q.B., Zhao, G.X., Hou, X.F., Shi, Z.J., Lin, Q.R., Ouyang, D.Y., He, X.H., 2015. Piperine metabolically regulates peritoneal resident macrophages to potentiate their functions against bacterial infection. Oncotarget 6, 32468–32483.

Park, B.S., Song, D.H., Kim, H.M., Choi, B.S., Lee, H., Lee, J.O., 2009. The structural basis of lipopolysaccharide recognition by the TLR4-MD-2 complex. Nature 458, 1191–1195.

Qureshi, S.T., Zhang, X., Aberg, E., Bousette, N., Giaid, A., Shan, P., Medzhitov, R.M., Lee, P.J., 2006. Inducible activation of TLR4 confers resistance to hyperoxia-induced pulmonary apoptosis. J. Immunol. 176, 4950–4958.

Rubenfeld, G.D., 2015. Confronting the frustrations of negative clinical trials in acute respiratory distress syndrome. Ann. Am. Thorac. Soc. 12, S58–S63. Suppl 1.

Shen, Y.J., Zhu, X.X., Yang, X., Jin, B., Lu, J.J., Ding, B., Ding, Z.S., Chen, S.H., 2014. Cardamonin inhibits angiotensin II-induced vascular smooth muscle cell proliferation and migration by downregulating p38 MAPK, Akt, and ERK phosphorylation. J. Nat. Med. 68, 623–629.

Shimazu, R., Akashi, S., Ogata, H., Nagai, Y., Fukudome, K., Miyake, K., Kimoto, M., 1999. MD-2, a molecule that confers lipopolysaccharide responsiveness on Toll-like receptor 4. J. Exp. Med. 189, 1777–1782.

Takahashi, A., Yamamoto, N., Murakami, A., 2011. Cardamonin suppresses nitric oxide production *via* blocking the IFN-gamma/STAT pathway in endotoxin-challenged peritoneal macrophages of ICR mice. Life Sci. 89, 337–342.

Tan, Y., Wan, H.H., Sun, M.M., Zhang, W.J., Dong, M., Ge, W., Ren, J., Peng, H., 2021. Cardamonin protects against lipopolysaccharide-induced myocardial contractile dysfunction in mice through Nrf2-regulated mechanism. Acta Pharmacol. Sin. 42, 404–413.

Tapping, R.I., Akashi, S., Miyake, K., Godowski, P.J., Tobias, P.S., 2000. Toll-like receptor 4, but not toll-like receptor 2, is a signaling receptor for Escherichia and Salmonella lipopolysaccharides. J. Immunol. 165, 5780–5787.

Wegiel, B., Larsen, R., Gallo, D., Chin, B.Y., Harris, C., Mannam, P., Kaczmarek, E., Lee, P.J., Zuckerbraun, B.S., Flavell, R., Soares, M.P., Otterbein, L.E., 2014. Macrophages sense and kill bacteria through carbon monoxide-dependent inflammasome activation. J. Clin. Invest. 124, 4926–4940.

Wei, Z., Yang, J., Xia, Y.F., Huang, W.Z., Wang, Z.T., Dai, Y., 2012. Cardamonin protects septic mice from acute lung injury by preventing endothelial barrier dysfunction. J. Biochem. Mol. Toxicol. 26, 282–290.

Yang, R.B., Mark, M.R., Gray, A., Huang, A., Xie, M.H., Zhang, M., Goddard, A., Wood, W.I., Gurney, A.L., Godowski, P.J., 1998. Toll-like receptor-2 mediates lipopolysaccharide-induced cellular signalling. Nature 395, 284–288.

Yu, W.G., He, H., Yao, J.Y., Zhu, Y.X., Lu, Y.H., 2015. Dimethyl cardamonin exhibits anti-inflammatory effects *via* interfering with the PI3K-PDK1-PKcalpha signaling pathway. Biomol. Ther. 23, 549–556.

Zhang, Y., Xu, T., Pan, Z., Ge, X., Sun, C., Lu, C., Chen, H., Xiao, Z., Zhang, B., Dai, Y., Liang, G., 2018. Shikonin inhibits myeloid differentiation protein 2 to prevent LPS-induced acute lung injury. Br. J. Pharmacol. 175, 840–854.